J Mater Sci (2007) 42:9807–9816
DOI 10.1007/s10853-007-1993-z

# Structural and chemical changes of thermally treated bone apatite

**Susan Essien Etok · Eugenia Valsami-Jones · Timothy J. Wess · Jennifer C. Hiller · Clark A. Maxwell · Keith D. Rogers · David A. C. Manning · Margaret L. White · Elisa Lopez-Capel · Matthew J. Collins · Mike Buckley · Kirsty E. H. Penkman · Stephen L. Woodgate**

Received: 5 October 2006 / Accepted: 13 July 2007 / Published online: 21 August 2007


**Abstract** The thermal behaviour of the animal by-product meat and bone meal (MBM) has been investigated in order to assess how it is affected structurally and chemically by incineration. Initially composed of intergrown collagen and hydroxyapatite (HAP), combustion of the organic component is complete by 650 °C, with most mass loss (50–55%) occurring by 500 °C. No original proteins were detected in samples heated at 400 °C or above. Combustion of collagen is accompanied by an increase in HAP mean crystallite size at temperatures greater than 400 °C, from 10 nm to a constant value of 120 nm at 800 °C or more. Newly formed crystalline phases appear beyond 400 °C, and include $\beta$-tricalcium phosphate, $NaCaPO_4$, halite (NaCl) and sylvite (KCl). Crystallite thickness as judged by small angle X-ray scattering (SAXS) increases from 2 nm (25–400 °C) to 8–9 nm very rapidly at 550 °C, and then gradually increases to approximately 10 nm. The original texture of HAP within a collagen matrix is progressively lost, producing a porous HAP dominated solid at 700 °C, and a very low porosity sintered HAP product at 900 °C.

S. E. Etok · E. Valsami-Jones (✉)
Department of Mineralogy, The Natural History Museum, Cromwell Road, London SW7 5BD, UK
e-mail: E.Valsami-Jones@nhm.ac.uk

T. J. Wess · J. C. Hiller · C. A. Maxwell
Biophysics Group, School of Optometry and Vision Sciences, Cardiff University, Cardiff CF10 3NB, UK

K. D. Rogers
Centre for Materials Science and Engineering, Cranfield University Shrivenham, Swindon SN6 8LA, UK

D. A. C. Manning · M. L. White · E. Lopez-Capel
School of Civil Engineering and Geosciences, Newcastle University, Newcastle upon Tyne NE1 7RU, UK

M. J. Collins · M. Buckley · K. E. H. Penkman
Bio-Arc (Archaeology), University of York, PO Box 373, York YO10 5YW, UK

S. L. Woodgate
PDM Group, c/o Beacon Research, Kelmarsh Road, Clipston, Leicestershire LE16 9RX, UK

## Introduction

The production of meat generates a range of by-products of animal origin, including bone. Bone, a natural composite material, comprises of nanocrystalline apatite mineral and fibrous protein. However, current EU legislation [1–3], severely restricts the use of meat and bone meal (MBM) in conventional applications such as animal feeds, in view of possible contamination by pathogenic components that may transmit diseases such as bovine spongiform encephalopathy (BSE). Some materials (category 1, [2]), are required to be heat treated to remove any potential BSE infectivity. Since land filling is not an option for disposal of MBM, the only alternative is thermal treatment using high temperature processes, typically using fluidised bed combustion [4–6], which have the benefit of recovering energy. There are possible uses for incinerated MBM; it has been proposed [6–8] that MBM combustion residue is an efficient low cost material for immobilisation of toxic metals in soil. However, feasibility studies are still in their infancy and further studies are required to ascertain the optimum mineral characteristics required to achieve a suitable rate of metal immobilisation. In addition few studies have detailed changes occurring in bone between nano- and macroscopic levels.

Identifying and understanding the heat-induced changes in bone is potentially valuable for resolving forensic and archaeological problems. In addition it has been reported [9, 10] that hydroxyapatite [$Ca_5 (PO_4)_3 OH$] material manufactured from mammalian bone sources has an advantage over synthetically produced analogues due to the fact that they inherit some of the structural and chemical properties of natural bone. Therefore, the extraction of HAP from bone sources could legitimately be exploited to provide an alternative for products based on synthetic HAP [10]. Possible applications include (i) feed powder for sprayed coatings for endoprostheses [11, 12], (ii) bone fillers and cements for orthopaedic surgery [13] and (iii) allograft or xenograft material [14, 15].

On heating, bone experiences extensive changes in structure and mineralogy. Kubisz et al. [16] have reported that heating bone up to 260 °C led to the removal of structural water, which according to the Ramachandran model [17] of degradation of collagen macromolecules, takes place when collagen changes its structure during denaturation. Collagen degradation was found to occur between 112 °C and 260 °C. Small angle X-ray scattering (SAXS) studies [18] have shown that bone mineral begins to alter within the first 15 min of heating at temperatures >500 °C and then stabilises to a temperature-specific thickness and shape with prolonged heating. Rogers et al. [9] have demonstrated that when heated at temperatures >800 °C, bone apatite crystals grow from a highly anisotropically strained state to one with significantly larger equidimensional crystals with little microstrain.

Several approaches for the investigation of the heat-induced changes occuring in bone have been proposed such as SAXS [19–21], X-ray diffraction (XRD) [9], porosimetry [20], spectroscopy [10], microscopy [10, 21, 22] and diagenetic indicators [23, 24]. Such studies have been limited to a few characterisation techniques and have therefore failed to interconnect the various stages of heat-induced transformation occurring in the mineral and organic phases.

In this study we have made a detailed structural characterisation of heat treated bone using a range of techniques that allow characterisation at different scales, using XRD and SAXS, combined with chemical and thermogravimetric analyses, in order to gain an in-depth understanding of the changes that occur in bone when heated.

## Methods and materials

### Sample preparation

Mammalian MBM was obtained from the PDM-Group, London factory.

The MBM was produced from Category 3 animal by-products that was processed (rendered) in accordance with the EU Animal By-Products Regulation (ABPR) [2]. The use of MBM produced is determined by both the EU ABPR and the EU Transmissible Spongiform Encephalopathy Regulation (TSER) [3]. In brief, mammalian animal by-product is reduced in size, and heated using indirect steam in a continuous processing cooker to >125 °C under atmospheric conditions. The elevated temperature causes moisture removal by evaporation, sterilisation of the material and release of fat from the fatty tissues. The processed material is pressed through an expeller press to yield a liquid fat (tallow) and a solid protein/ mineral material termed MBM. The category 3 MBM produced at this location typically has the following analysis: Crude Protein ~55%, Fat ~12%, Ash ~25% and Moisture <5%. The calorific value of MBM is ~24 MJ/kg.

A systematic series of test samples was prepared by heating 50 g of MBM in air at temperatures of 400 °C, 500 °C, 550 °C, 600 °C, 650 °C, 700 °C, 750 °C, 800 °C, 850 °C and 900 °C (at a rate of 30 °C*$min^{-1}$) for 6 h in an electric furnace (Carbolite 1100). After heat treatment, the samples were air cooled and placed into a desiccated storage vessel at room temperature in accordance with Rogers et al. [9].

### Characterisation

X-ray diffraction analysis was carried out at the Natural History Museum (NHM) using a Philips PW1830 diffractometer with a diffracted beam monochromator to produce diffractograms from CuK$\alpha$ wavelengths. The test samples were mounted onto a low background diffraction support. Data was collected in the 10° to 100°/2$\theta$ range with a step size of 0.02°/2$\theta$ and a count time of 20 s. Phase identification was performed with reference to the database supplied by the International Centre for Diffraction Data using the software, 'CSM' (Oxford Cryosystems). Whole pattern fitting was undertaken using Topas academic (Bruker-AXS) [25] as described in previous work [11, 12]. Atomic structural parameter values were acquired from Inorganic Crystal Structure Database. In this analysis, the background shape was determined empirically using data from the sample holder and this was represented as a 1st order polynomial. In all refinements scale factors, lattice parameters and peak shapes were refined for all crystalline phases. Long data collection times and small step sizes were employed to obtain high quality data and hence reduce correlations between variables. For microstructural analysis, the double-Voigt approach [26] was employed using Topas academic [25]. Only the (002) peak was

exploited in this analysis due to severe peak overlap associated with biological apatite [9, 27].

For SAXS analysis, 1.5 mg of test sample was loaded into a specially designed sample carriage between two mica sheets and then attached to the stage. The stage was mounted into a vacuum chamber of the NanoSTAR (Bruker AXS, Karlsruhe) X-ray facility at Cardiff University, which uses a SAXS sample-to-detector distance of 1.25 m. The data collection procedure used followed that described in detailed by Wess et al. [19]. The data collected was corrected for camera distortions, a background image subtracted, and images were analysed using in-house software. The two-dimensional detector output was converted into spherically averaged one-dimensional profiles. Hence values for crystal thickness (T) of the smallest dimension can be determined from the SAXS data. A detailed procedure for these calculations is described elsewhere [27, 28].

Thermal analysis (thermogravimetric analysis [TGA], quantitative mass spectrometry [QMS] and differential scanning calorimetry [DSC]) of the heated specimens was carried out using a Netzsch Simultaneous Thermal Analyzer (STA 449C Jupiter) equipped with a TG-DSC sample carrier (type S supporting a $Pt_{90}Rh_{10}$-Pt thermocouple) at the University of Newcastle. 30 mg of test sample was heated in an alumina crucible at a rate of 10 °C $min^{-1}$ from 25 °C–1,000 °C. The combustion gas (20% $O_2$; 80% He) was circulated through the combustion chamber at a flow rate of 50 mL/min. Rat-tail collagen (Cranfield University, Shrivenham, UK) and synthetic apatite (Fluka, UK) were used as reference materials.

Morphological analysis of the test samples was carried out using scanning electron microscopy (SEM; Leo XL-30 SEM) at the NHM. Prior to analysis, test samples were sputter coated with a gold-palladium alloy to prevent charging. Fourier transform infrared spectroscopy was carried out using a Perkin–Elmer spectrum 1 in transmission mode on KBr discs, scanning the 4,000–400 $cm^{-1}$ region using 50 scans with a spectral resolution of 2 $cm^{-1}$.

Amino acid racemisation analyses of the test samples were conducted at York University as follows. The bone powder was treated with 7 M HCl under $N_2$ at 110 °C for 18 h to demineralise the hydroxyapatite and release any peptide-bound amino acids, thus yielding the 'total' amino acid concentration. Samples were then dried with a centrifugal evaporator and rehydrated for RP-HPLC analysis with 0.01 mM L-homo-arginine as an internal standard. The amino acid compositions were analysed in duplicate by RP-HPLC using fluorescence detection, following a modified method of Kaufman et al. [29]. A 2 mL sample was injected and mixed online with 2.2 mL of derivitizing reagent (260 mM *n*-iso-Lbutyryl L-cysteine (IBLC) and 170 mM *o*-phthaldialdehyde (OPA) in 1 M potassium borate buffer, adjusted to pH 10.4 with potassium hydroxide pellets). The amino acids were separated on a C18 HyperSil BDS column (5 mm × 250 mm) at 25 °C with a gradient elution of three solvents: sodium acetate buffer (solvent A; 23 mM sodium acetate tihydrate, 1.5 mM sodium azide, 1.3 mM EDTA, adjusted to pH 6.00 ± 0.01 with 10% acetic acid and sodium hydroxide), methanol (solvent C) and acetonitrile (solvent D). The L and D isomers of ten amino acids were routinely analysed. During preparative hydrolysis both asparagine and glutamine undergo rapid irreversible deamination to aspartic acid and glutamic acid, respectively [30]. It is therefore not possible to distinguish between the acidic amino acids and their derivatives and they are all reported together as Asx and Glx respectively.

## Results

Figure 1 presents X-ray diffractograms for a series of heated test samples. The as-received MBM has the characteristic broad Bragg maxima associated with poorly crystalline materials. An increased background hump was observed in the 15°–30°/2$\theta$, which has been reported to be due to the organic component of bone [9]. After heating at 400 °C the background hump is not visible. Between 400 °C and 700 °C, there is marked decrease in peak width (Figs. 1, 2) and peaks become well resolved. The principal mineral phase identified corresponded to bone apatite, however at heating temperatures above 500 °C, low

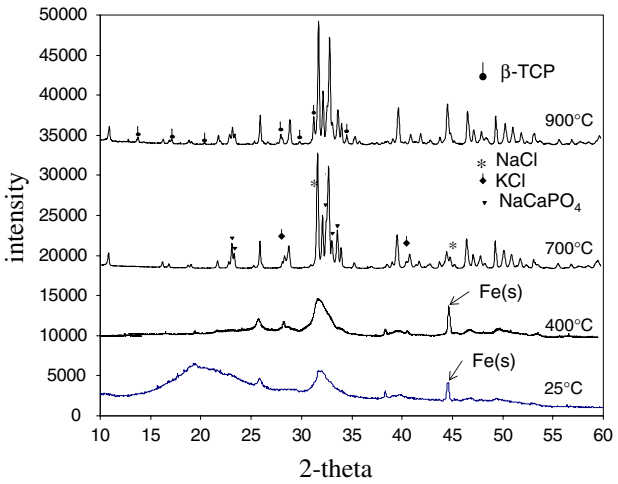


**Fig. 1** Diffraction data for heat-treated MBM samples. At 25 °C and 400 °C an arrow marks the position of crystalline Fe(s), probably an impurity from the milling process. At 700 °C arrowheads (▼), diamonds (♦) and asterisks (*) mark $NaCaPO_4$, sylvite (KCl) and halite (NaCl) respectively. All other unmarked peaks correspond to apatite. At 900 °C one additional phase is identified, $\beta$-TCP. All other unmarked peaks on this pattern are the same as at 700 °C

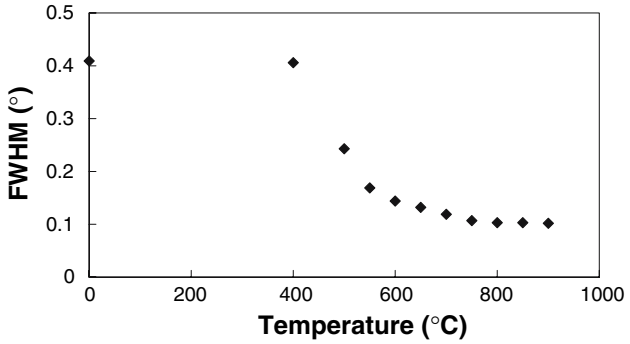


**Fig. 2** FWHM (peak width) of (002) as function of heating temperature

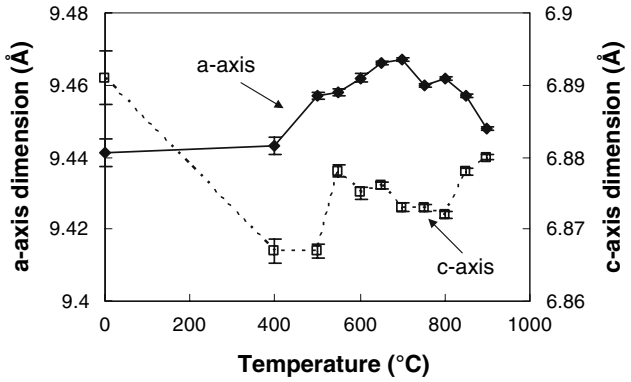


**Fig. 3** Lattice parameter changes as a function of heating temperature

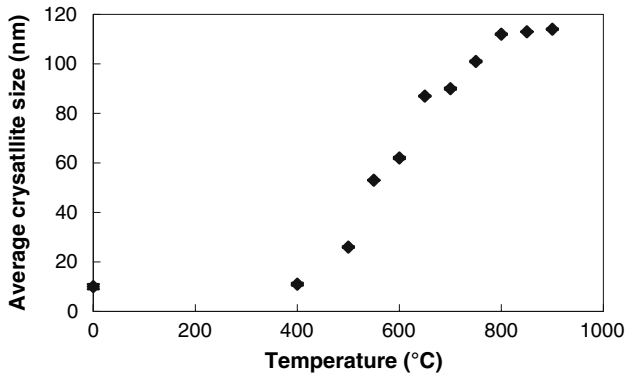


**Fig. 4** Changes in the average crystallite size as a function of heating temperature

intensity peaks corresponding to additional phases were discernible. In addition to apatite, $NaCaPO_4$, KCl and NaCl were observed between 500 °C and 900 °C (Table 1) and $\beta$-tricalcium phosphate ($\beta$-TCP) in specimens heated at 900 °C.

Figure 3 depicts the changes in '*a*' and '*c*' axis lattice dimensions with heating temperature. The lattice parameters of the as-received MBM are consistent with previous work [9] on human cortical bone. On heating at 400 °C, the *a*-axis dimension does not differ significantly from the *a*-axis parameter of the as-received MBM. With increasing temperature of heating, the *a*-axis dimension steadily increases reaching a maximum at 650 °C and then decreases reaching a minimum at 900 °C. The *c*-axis dimension decreases on heating MBM at 400 °C and then remains steady until 600 °C and increases reaching a maximum at 900 °C.

The values of average crystallite size of heated samples was determined adopting the double-Voigt approach [26] , separating the peak broadening contributions from crystallite size and lattice microstrain (Fig. 4). The crystallite sizes reported here represent volume weighted column heights in the <002> direction. As the heating temperature increases, the crystallite size increases reaching a plateau at 800 °C (114 nm). Interestingly, the crystallite size corresponding to the sample heated at 400 °C (11 nm) was not significantly different from the as-received MBM (10 nm). The largest increase in crystallite size was observed when the MBM specimens were heated between 400 °C and 650 °C.

**Table 1** Crystalline phases present in combustion residue

| Temperature (°C) | Phases present |
|---|---|
| 25 | HAP |
| 400 | HAP |
| 500 | HAP, $NaCaPO_4$, KCl, NaCl |
| 550 | HAP, $NaCaPO_4$, KCl, NaCl |
| 600 | HAP, $NaCaPO_4$, KCl, NaCl |
| 650 | HAP, $NaCaPO_4$, KCl, NaCl |
| 700 | HAP, $NaCaPO_4$, KCl, NaCl |
| 750 | HAP, $NaCaPO_4$, KCl, NaCl |
| 800 | HAP, $NaCaPO_4$, KCl, NaCl |
| 850 | HAP, $NaCaPO_4$, KCl, NaCl |
| 900 | HAP, $NaCaPO_4$, $\beta$-TCP, KCl, NaCl |

The XRD analyses measure the *c*-axis of the crystallites; by comparison, SAXS was used to investigate the thickness of the crystallites in the smallest (ab) dimension. The SAXS data (Fig. 5) reveal changes in the crystallite form, including habit and size, of the mineral phase as a function of temperature. With increased heating, the shape of the SAXS curves indicates that crystallites, which are large in the ab plane, are evolving, with the mean thickness in the smallest dimension changing from 2.5 nm to $\geq$10 nm (Fig. 6). The scattering curves also indicate that a large range of crystallite shapes is present in the samples heated to higher temperatures, as the physiological platelet shape is lost. In the results obtained in our experiments, crystallite thickness measurements were observed to increase substantially with higher temperature heating regimes, a result consistent with previous findings [19]. The primary change

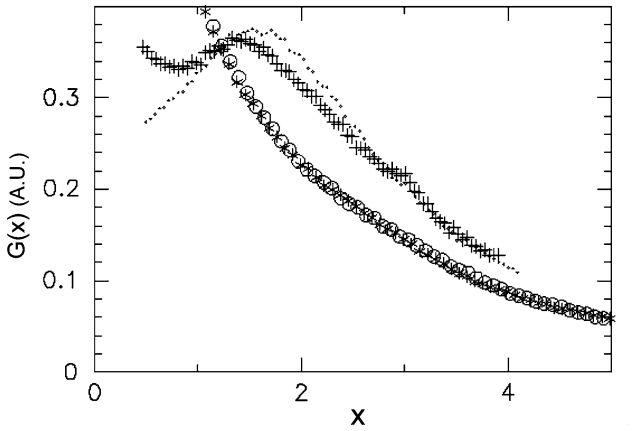


**Fig. 5** Image of scattering curves from unheated (dots (·) and crosses (+)) and 400 °C heated (asterisks (*) and circles (○)) bone meal. The curves have been rescaled to a parameter X (=qT) that removes the contribution of crystallite thickness and renders the shape parameter dimensionless. The control bone meal (dots and crosses) show the platelet shape typical of physiological crystallites, while the heated samples show a polydisperse crystallite habit

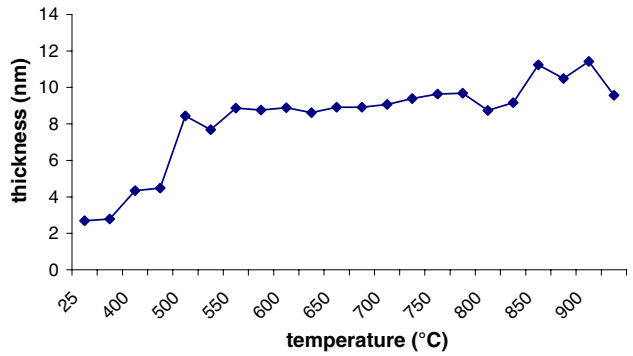


**Fig. 6** Graph showing variation in crystal thickness with increasing temperature

occurs at 500 °C, where the crystallites suddenly double in size from the thicknesses recorded at 400 °C. Subsequently, the crystallite thickness increases in a mostly linear fashion (Fig. 6), until the highest temperatures (>700 °C), when the measurements become increasingly variable. This may be due to the nature of the sample at higher temperatures, or with the limitations of a laboratory-based SAXS apparatus at measuring crystallite thicknesses in excess of 10 nm.

Figure 7 depicts FTIR spectra of the as-received and heat treated samples. Prior to heat treatment, the spectra corresponding to the as-received bone meal sample were broad and featureless corresponding to a typical spectrum of natural bone [31]. No clear peaks corresponding to apatite or collagen are discernible due to severely overlapping bands and poor crystallinity. With an increase in thermal treatment temperature there is also an increase in resolution of the bands at 500–700 $cm^{-1}$ (this has been employed previously by Etok et al. [12] as a 'splitting factor' to characterise apatites). The FTIR spectra corresponding to samples heated at 400 °C and above were consistent with spectra corresponding to synthetic carbonated hydroxyapatite [12, 32–33]. Above 700 °C, the intensity of the $OH^-$ signal at 3,400 $cm^{-1}$ increases as thermal treatment temperature increases. No $OH^-$ signal is visible in the heated samples until the heating temperature reaches 700 °C. In addition there is a progressive decrease in the area of the bands at 1,300–1,500 $cm^{-1}$ with increase of thermal treatment temperature. The bands at 1,300–1,500 $cm^{-1}$ have previously been assigned to lattice carbonate [12]. The increase in the $OH^-$ signal and decrease in the area of the carbonate bands with thermal treatment temperature suggests that A-type carbonate substitution is decreasing and $OH^-$ ions are replacing $CO_3^{2-}$. This is consistent with previous work by Haberko et al. [10].

The percentage weight loss of the MBM specimens with heating temperature are illustrated in Fig. 8. The greatest weight loss was observed when the MBM specimens are heated to 500 °C (∼60 wt.%). This is followed by a steady increase in weight loss, which reaches a plateau between 650 °C and 900 °C. This plateau region is consistent with TG-DSC data (Fig. 9), which show that no net weight loss occurred after 650 °C, at which point the sample had lost 70% of its original mass. TG-DSC data also show the temperature range that is associated with maximum loss in weight is 280–400 °C.

In detail, TG data show a weight loss (∼7 wt.%) between 20 °C and 250 °C, which corresponds with a broad endothermic peak, initially due to evaporation of moisture [10] but also including loss of structurally bound water following denaturation of proteins, which in the case of mineralised collagen occurs between 130 °C and 170 °C (Collins, unpublished data; Kronick et al. 1995). There is an intense single exothermic peak at ∼590 °C and a less intense doublet at ∼380–400 °C (Fig. 9). These exothermic peaks have previously been assigned to as being due to the combustion of the organic material [6] and are consistent with TG-DSC data for collagen from previous work [35].

Analysis of evolved gases during thermogravimetric testing revealed $H_2O$ emissions at ∼70 °C and 296–381 °C; $CO_2$ emissions at ∼380 °C and ∼600 °C reflecting the combustion of the char; CN emissions at ∼380 °C and ∼470 °C; $NO_2$ emissions at ∼300 °C and ∼600 °C; and $SO_2$ emissions at ∼380 °C. Similar observations have been made by Lozano et al. [35]. No further gas evolution was observed above ∼650 °C, hence it is plausible that under the conditions of this experimental work combustion was complete by ∼650 °C (Fig. 10).

The amino acid data reveal large amounts of peptide bound amino acids in the 'as received' samples.

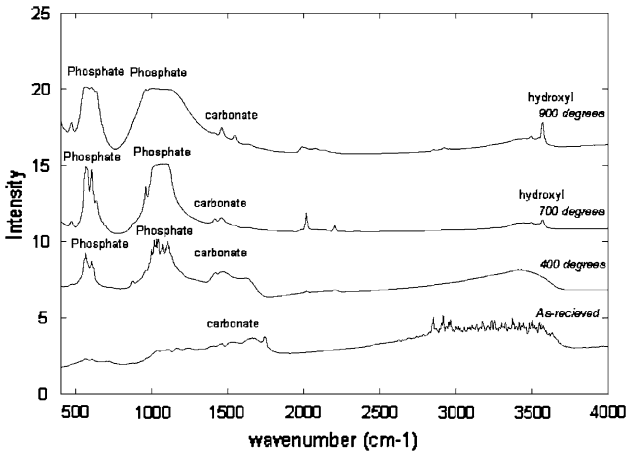


**Fig. 7** FTIR spectra of heat treated MBM samples

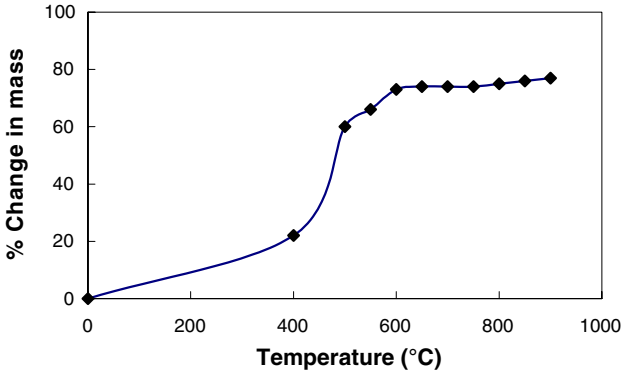


**Fig. 8** Percentage change in mass of MBM as a function of heating temperature

Unsurprisingly, in a product used as a protein feedstock, amino acids persist in the 'as received' MBM sample after the dehydration (at 110 °C for 4–5 h) and sterilisation steps (133 °C for 20 min/3 Bar). However the thermal pretreatment is indicated by higher than in vivo levels of accumulated D- amino acids (Table 2). In all heated samples (i.e. 400 °C and above) amino acid levels are below detection limits (2 SD of blanks). At 600 °C a new fluorescent peak eluted at approximately the same position as L-Ile in the "as received" sample (81 min) but at an intensity three orders of magnitude lower, the yield of this peak declining with temperature. It is not known what this compound is, but the low activation energy (13.8 kJ $mol^{-1}$; $n = 5$, $R^2 = 0.99$) for the temperature dependent loss of the peak suggests that it may represent the thermal desorption of a (fluorescent) decomposition product derived from the heating.

SEM micrographs of the heated MBM samples are presented in Fig. 11a–d. The as-received MBM samples comprise of small mineral crystals embedded in an organic (collagen) matrix. At 400 °C, increased porosity was noticeable, which is due to the denaturation and shrinkage of the collagen matrix. By 700 °C, the collagen matrix is not present and the mineral crystals have increased in relative size (0.5–4.5 μm). As a result of the complete degradation and combustion of the collagen matrix, there is a marked increase in surface porosity in the samples heated at 700 °C compared to the samples heated at 400 °C. However the crystals had fused in localised areas. The mineral crystals produced at 900 °C are approximately 1.25–7.5 μm in size with a hexagonal morphology. No surface porosity is visible, as the crystals had fused. The observations made in the SEM micrographs corroborate the findings of the XRD and TG-DSC analysis.

## Discussion

The crystalline phases identified in the heated specimens in this study are consistent with a previous study [5] of MBM combustion residue. The most significant structural changes in the crystalline phase occur between 500 °C and 700 °C. At heating temperatures <500 °C, there is no net change in the crystallite size and thickness. When heated to ~500 °C, both the crystallite size (XRD) and thickness (SAXS) double in magnitude. This change in microstructure is accompanied by the formation of extraneous phases such as $\beta$-TCP, which is due to the partial thermal degradation of natural apatite. Whilst other authors [9, 10, 35] have reported the presence of CaO in the combustion residue (>700 °C), this is ascribed to the differences in the species of donor bone and the heating process.

The onset of phase transformations and changes in microstructure at ~500 °C suggest that prior to this temperature, the mineral phase is not affected by the thermal treatment. From the thermogravimetric and amino acid data, it has been shown that ~500 °C, complete degradation and combustion of the more labile organic phase of MBM (50–55% of the organic component) has occurred (later weight loss involves the combustion of more refractory organic material, including char produced artificially during the heating experiment). This suggests that on heating, the changes in the mineral phase of the MBM occurred once the original organic component has been removed; hence the organic bone matrix has a 'thermal shielding effect' that protects the texture of the mineral phase. The degradation and decomposition of the restrictive collagen fibrils then releases the nanocrystallite mineral surfaces and encourages sintering at higher temperatures.

Previous research [36, 37] on heat treated human bone has shown that the fundamental architecture of bone is

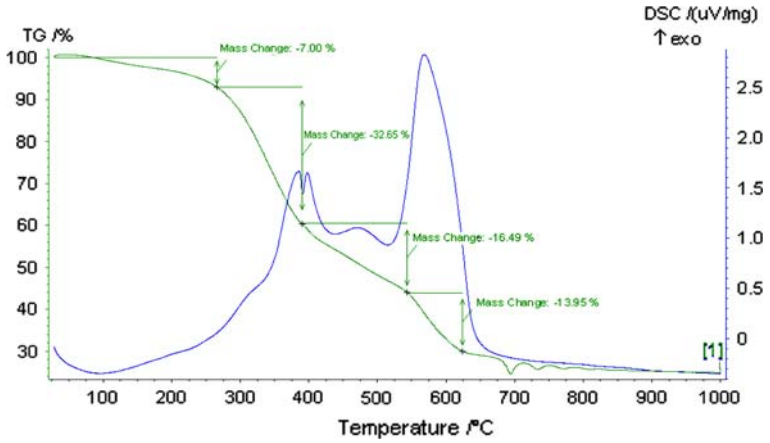


**Fig. 9** Thermogravimetric analysis of a typical MBM sample, showing locations of main mass changes

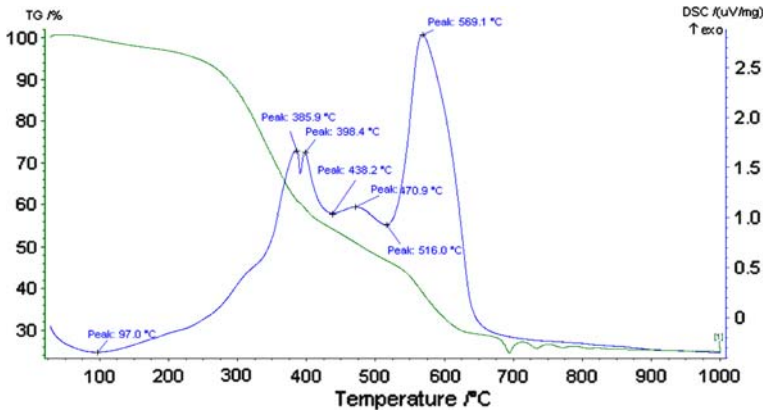


**Fig. 10** Differential scanning calorimetry data of a typical MBM sample, as in Fig. 9, this time showing temperature peak assignment

preserved even at temperatures a high as ~500 °C despite the absence of bone proteins constituents such as the collagen amino acid hydroxyproline. Likewise, in this study, Fig. 11b, an SEM micrograph of a MBM sample heated at 400 °C shows morphological evidence of an organic matrix despite the amino acid data suggesting that no proteins are present. Above ~600 °C (Fig. 11c–d), this feature is no longer discernible.

Thermal analysis experiments [35] have shown that extracted bone collagen has a higher thermal stability than when still mineralised. The higher stability following mineralisation is explained by the fact that mineral crystals act as fracture centres. Therefore the absence of these fracture centres following demineralisation results in higher thermal stability. In addition, it has been suggested that a denatured collagen fibril does not transform to its original conformation prior to heat treatment, but intertwines with other collagen molecules giving rise to a different structure. It is possible that the resultant structure contains a large number of secondary bonds as a result of closer interactions with molecules [35]. In natural bone protein secondary bonds are present as interface between organic and inorganic phases (gap regions). The secondary bonds have a significant influence on the interaction of the organic and inorganic phases. Lozano et al. [35] have postulated that if gap density is proportional to the area/volume ratio, then the interfaces may influence the thermal stability of the proteins.

According to the XRD data (Fig. 4), significant crystallite size growth occurs between 400 °C and 700 °C. However, of note is the fact that the double-Voigt method employed in this study provides a weighted, spatial average of crystallite size estimates. Therefore as noted by Rogers et al. [9], the observed crystallite size growth may indeed represent changes in crystallite distribution as a result of preferential resorption of smaller crystallites. At temperatures >800 °C, the 'apparent' crystallite size (within experimental error) remains constant which is in accord with previous work [9].

The 'c' lattice parameters of the samples heated at ~400 °C show a 0.3% decrease in magnitude with respect to the as-received MBM. This decrease in magnitude may be due to ionic exchange in the mineral phase resulting from the degradation and combustion of the organic phase and water loss. No net change in the 'a' lattice parameter (within experimental error) is observed until the samples are heated to ~500 °C. Between 400 °C and 700 °C, there is a 0.3% increase in the 'a' lattice parameter and 0.2% decrease in the 'c' lattice parameter. This is perhaps partly due to the exclusion of lattice carbonate from the $OH^-$ sites

**Table 2** (a) Amino acid concentrations of heated MBM samples (nanomoles per milligram). (b) Amino acid D/L values of heated MBM

| (a) | | | | | | | | | | | |
|---|---|---|---|---|---|---|---|---|---|---|---|
| Sample | Asx | Glx | Ser | Thr | Gly | Arg | Ala | Val | Phe | Leu | Ile |
| 130°C | 379.50 | 571.87 | 239.28 | 195.21 | 1528.33 | 240.69 | 536.36 | 249.05 | 144.67 | 380.01 | 182.96 |
| 400 | – | – | – | – | – | – | – | – | – | – | – |
| 450 | – | – | – | – | – | – | – | – | – | – | – |
| 500 | – | – | – | – | – | – | – | – | – | – | – |
| 550 | – | – | – | – | – | – | – | – | – | – | – |
| 600 | – | – | – | – | – | – | – | – | – | – | – |
| 650 | – | – | – | – | – | – | – | – | – | – | – |
| 700 | – | – | – | – | – | – | – | – | – | – | – |
| 750 | – | – | – | – | – | – | – | – | – | – | – |
| 800 | – | – | – | – | – | – | – | – | – | – | – |
| 850 | – | – | – | – | – | – | – | – | – | – | – |
| 900 | – | – | – | – | – | – | – | – | – | – | – |

| (b) | | | | | | | | | |
|---|---|---|---|---|---|---|---|---|---|
| Sample | Asx | Glx | Ser | Arg | Ala | Val | Phe | Leu | Ile |
| 130°C | 0.10 | 0.04 | 0.00 | 0.06 | 0.03 | 0.01 | 0.03 | 0.03 | 0.07 |
| 400 | – | – | – | – | – | – | – | – | – |
| 450 | – | – | – | – | – | – | – | – | – |
| 500 | – | – | – | – | – | – | – | – | – |
| 550 | – | – | – | – | – | – | – | – | – |
| 600 | – | – | – | – | – | – | – | – | – |
| 650 | – | – | – | – | – | – | – | – | – |
| 700 | – | – | – | – | – | – | – | – | – |
| 750 | – | – | – | – | – | – | – | – | – |
| 800 | – | – | – | – | – | – | – | – | – |
| 850 | – | – | – | – | – | – | – | – | – |
| 900 | – | – | – | – | – | – | – | – | – |

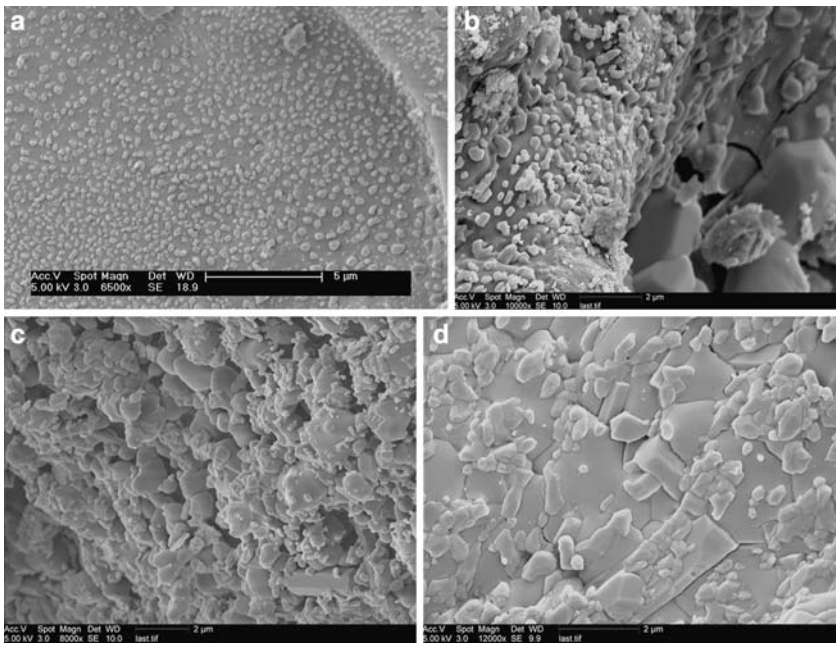


**Fig. 11** SEM micrograph of: (**a**) as-received MBM. (**b**) MBM after heat treatment at 400 °C. (**c**) MBM after heat treatment at 700 °C. (**d**) MBM after heat treatment at 900 °C

as evidenced by the FTIR data. Rogers et al. [9] have reported similar findings and have concluded that no single ionic exchange mechanism can account for the magnitude and direction of these lattice parameter changes nor the lower temperature of change in the 'c' parameter compared to the 'a' parameter.

## Conclusions

This study is a comprehensive investigation of the thermally induced changes occurring in the organic and mineral phases of bone. There are three key stages through which MBM passes as it is heated:

(1) 25–250 °C: loss of loosely bound water up to 100 °C, with little change in organic and mineral matrices, followed by loss of structural water within protein and mineral-surface bound water up to 250 °C.
(2) 300–500 °C: combustion of organic component (50–55% mass loss), associated with increase in mean crystallite size from 10 nm to 30 nm, and an increase in crystallite thickness from 2 nm to 8–9 nm, together with formation of new mineral phases ($NaCaPO_4$, halite, sylvite). A proportion of the organic matter likely forms a char. Amino acids were below detection.
(3) above 500 °C: any residual organic matter, including char, is burnt off, and mean crystallite size progressively increases to a constant value of 110 nm at 800 °C. Crystallite thickness increases gradually to approximately 10 nm. Having lost intergrown organic matter, the mineral component forms an open porous texture that condenses on sintering and is lost by 900 °C, when a closely interlocking texture is produced. A further phase, $\beta$-tricalcium phosphate, appears at 900 °C.

From the point of view of considering new applications for incinerated MBM, this study has shown that all organic matter is destroyed by 650 °C. There are no detectable original amino acids in samples heated to 400 °C or more, and it appears that the original organic matter is combusted by 500 °C, in the process forming a char during laboratory analysis. This char may be absent from industrial incineration systems, depending on combustion characteristics.

Mineralogically, combusted MBM is very simple. The physical properties of the combusted MBM depend on the temperature of combustion, and this will affect its suitability for specific end uses.

**Acknowledgements** This study was sponsored by NERC (Grant no: NERD/S/2003/00678) and the PDM Group. The authors wish to thank Martin Gill and Gordon Cressey for their invaluable assistance with XRD analysis and interpretation respectively. In addition thanks go to Mr. Gary Jones for his assistance with FTIR measurements.

## References

1. Conditions for the production of MBM and tallow. In: (1999/534/EC) Council decision of 19 July 1999
2. Laying down health rules concerning animal by-products not intended for human consumption. In: Regulation (EC) No 1774/2002 of the European Parliament and of the Council (LS73/1). 2002
3. Laying down rules for the prevention, control and eradication of certain transmissible spongiform encephalopathies. In: Regulation (EC) No 999/2001 of the European Parliament and of the Council (L147/1). 1999
4. Cyr M, Ludmann C (2006) Cement Concrete Res 36(3):459
5. Deydier E, Guilet R, Sarda S, Sharrock P (2005) J Hazard Mater B121:141
6. Deydier E, Guilet R, Sharrock P (2003) J Hazard Mater B101:55
7. Valsami-Jones E, Ragnarsdottir KV, Putnis A, Bosbach D, Kemp AJ (1998) Chem Geol 151(1–4):215
8. Knox AS, Kaplan DI, Paller MH (2006) Sci Total Environ 357 (1–3):271
9. Rogers KD, Daniels P (2002) Biomaterials 23:2577
10. Haberko K, Bucko M, Brzezinska-Miecznik J, Haberko M, Mozgawa W, Panz T, Pyda A, Zarebski J (2006) Euro Ceram Soc 26:532
11. Rogers KD, Etok SE, Scott R (2004) J Mater Sci 39:5747
12. Etok SE, Rogers KD, Scott R (2005) J Mater Sci 40(21):5627
13. Fernandez E, Gil F, Ginebra MP, Driessens FC, Planell JA (1999) J Mater Sci: Mater Med 10:169
14. Guizzardi S, Montanari C, Migliaccio S, Strocchi R, Solmi R, Martini D, Ruggeru A (2000) J Biomed Mater Res 53:227
15. Catanese J, Featherstone J, Keaveny T (1999) J Biomed Mater Res 45:327
16. Kubisz L, Mielcarek S (2005) J Non-Cryst Solids 351:2935
17. Ramachandran G (1988) Int J Peptide Res 31(1):1
18. Hiller JC, Thompson TJU, Evison MP, Chamberlain AT, Wess TJ (2003) Biomaterials 24:5091
19. Wess TJ, Alberts I, Hiller J, Chamberlain AT, Drakopoulos M, Collins M (2002) Calcif Tissue Int 70(2):103
20. Thompson TJU (2004) Forensic Sci Int 146S:S203
21. Zizak I, Roschger P, Paris O, Misof BM, Berzalanovich A, Bernstorff S, Amenitsch H, Klaushofer K, Fratzl P (2003) J Struct Biol 141:208
22. Koon HEC, Nicholson RA, Collins MJ (2003) J Archaeol Sci 30:1393
23. Roberts SJ, Smith CI, Millard A, Collins MJ (2002) Archaeometry 44(3):485
24. Holmes KM, Robson-Brown KA, Oates WP, Collins MJ (2005) J Archaeol Sci 32(2):157
25. Coelho R (ed) (2003) Users manual: topas academic. Bruker-AXS, Karlsruhe
26. Danilchenko SN, Moseke C, Sukhodub LF, Sulkio-Cleff B (2004) Crystal Res Technol 1:71
27. Fratzl P, Groschner M, Vogl G, Plenk H, Eschberger J, Fratzl-Zelman N, Koller K, Klaushofer K (1992) J Bone Miner Res 7(3):329
28. Fratzl P, Screiber S, Klaushofer K (1996) Connect Tissue Res 34(4):247
29. Kaufman DS, Manley WF (1998) Quatern Sci Rev (Quaternary Geochronology) 17:987
30. Hill RL (1965) Adv Protein Chem 20:37

31. Miller LM, Vairavamurthy V, Chance MR, Mendelsohn R, Paschalis EP, Betts F, Boskey AL (2001) Biochimica et Biophysica Acta 1527(1–2):11
32. Etok SE (2005) Structural characterisation and in vitro behaviour of apatite coatings and powders. In: PhD thesis, Department of Materials & Medical Sciences, Cranfield University, Shrivenham, UK
33. Gibson IR, Bonfield W (2002) J Biomed Mater Res 59(4):697
34. Sampath Kumar TS, Manjubala I, Gunasekaran J (2000) Biomaterials 21(16):1623
35. Lozano LF, Pena-Rico MA, Heredia A, Octolan-Flores J, Gomez-Cortes A, Velazquez R, Belio IA, Bucio L (2003) J Mater Sci 38:4777
36. Holden JL, Phakey PP, Clement JG (1995) Forensic Sci Int 74:29
37. Raspanti M, Guizzardi S, DePasquale V, Martini D, Ruggeri A (1994) Biomaterials 15:433